Computers and Concrete, *Vol. 12, No. 5 (2013) 717-737*
DOI: http://dx.doi.org/10.12989/cac.2013.12.5.717

A study on the fire performance and heat transfer of the HPC column with fiber-cocktail in ISO fire under loading condition

Hyung-Jun Kim[1a], Heung-Youl Kim[1b], In Kyu Kwon[*2], Ki-Hyuk Kwon[3c],
Byung-Yeol Min[1d] and Bum-Yean Cho[1e]

[1]Fire Saftey Research Center, Korea Institute of Construction Technology, Korea
[2]Department of Fire Protection Engineering, Kangwon National University, Korea
[3]Department of Architectural Engineering, University of Seoul, Korea

(*Received April 25, 2012, Revised August 6, 2013, Accepted August 31, 2013*)

Abstract. In this study, experiment and numerical analysis were conducted to identify the heat transfer characteristics and behavior of high-strength concrete upon a fire. The numerical analysis was employed to forecast the characteristics and properties of the high-strength concrete upon a fire, which can not be accomplished through a fire test due to the specific conditions and restrictions associated with the test. The result of the numerical analysis was compared with that of the test to verify the reliability of the analysis. In the numerical analysis of the heat transfer characteristics and behavior of 80 and 100 MPa high-strength concrete upon a fire, the commercial software of ABAQUS(V.6.8) was used. It was observed from the experiment that the contraction of the concrete with fiber-cocktail was mitigated by 25~55 % compared with that without fiber-cocktail because the fiber controlled the heat transfer of the concrete and thus improved the fire-resistance performance of the column.

Keywords: high strength concrete; heat transfer; fire performance; fiber-cocktail; spalling

1. Introduction

As supertall buildings have been built, concrete has gotten stronger. Along with the development of the technology for high-strength concrete, the requirement for functionally reliable fire-resistance design has increased to secure the fire performance of the high-strength concrete applied to supertall building upon a large-scale fire. High-strength concrete is vulnerable to spalling when exposed to high temperatures since the temperature difference between outside and inside the concrete causes thermal stress and the pore pressure inside the concrete rises rapidly due to its lower water permeability and higher density compared to generic concrete. (Lee 2009)

*Corresponding author, Professor, E-mail: kwonik@kangwon.ac.kr
[a]Researcher, E-mail: kimfestival@kict.re.kr
[b]Fellow Researcher, E-mail: hykim @kict.re.kr
[c] Professor, E-mail: kwonik@kangwon.ac.kr
[d]Fellow Researcher, E-mail: bymin@kict.re.kr
[e]Researcher, E-mail: choby277@kict.re.kr

http://www.techno-press.org/?journal=cac&subpage=8 ISSN: 1598-8198 (Print), 1598-818X (Online)

Therefore, the studies on functional fire-resistance design technology should be conducted to secure the structural safety of supertall buildings employing high-strength concrete upon a fire (Park 2010).

While fire tests and the studies on analysis methods have been made in the countries advanced in fire-resistance for the last 30 years in an attempt to develop the technology for fire-resistance design, the achievement made in Korea is not noticeable. The high costs, in particular, inherent in full-scale fire tests make it practically infeasible to conduct the tests repeatedly, so the analyses of temperature distribution and thermal stress distribution associated with different cross-sections have not been made enough to provide fire-resistance design based on structural performance (Lee 2008). Therefore, the development of fire-resistance design technology to mitigate spalling upon a fire is required to employ high-strength concrete members. (Eurocode 3 1995, Eurocode 4 1994) Thus, the case study (Kim 2007) of the experimental studies on spalling conducted in advanced countries and the influential factors on spalling and controlling methods preceded in order to analyze the influence of high-strength concrete on its spalling and decide the way to mitigate it (Anderberg 1997, Franssen 2000, Jumpannen 1989, Kodur 1998, Lie 1994).

In this study, the improvement in the thermal characteristics and behavior of structure at high temperatures achieved by the fiber-cocktail used to improve the fire-resistance performance of high-strength concrete columns was examined and the numerical analysis of the temperature changes and axial deformation of steel bars in the high-strength concrete columns was conducted to analyze the heat transfer characteristics and fire behavior of the high-strength concrete columns upon a fire. The information from existing data and the results of the material test conducted in this study were used as the input data for the numerical analysis and the result of the numerical analysis of the high-strength concrete was compared with the test result. (Purkiss 1996, Morris 1998).

2. Test variables & input data

Fire test and analysis of the specimens made of 40~60 MPa concrete were conducted simultaneously in order to analyze the fire behavior of the high-strength concrete columns and the results were compared to verify the reliability of the analysis method. The analysis method verified through the comparison with the test result was applied to the prediction of the fire behavior of 80~100 MPa high-strength concrete columns.

2.1 Selection of test variables & mixture design

When exposed to high temperatures, the structural members made of high-strength concrete experience the damage to cross-sections due to concrete spalling and falling, the steel bars of the members are exposed to the fire and the fire-resistance performance of the concrete members deteriorates seriously enough to lose their structural function (Hertz 2003, Harada 1972, Ashkan *et al.* 2011).

Though the most economically-efficient way of using polypropylene (more than 1.5 kg/m^3, 10～20 mm in length, 50～200 μm in diameter) was considered, the material test showed strength deterioration in high-strength concrete(Phan 2002, Kim 2010). Then, the material test of the fiber-cocktail where the polypropylene controls spalling and steel fiber prevents cracking and falling was conducted(Yousef 2011). Specimens for the test and numerical analysis of the high-strength

Table 1 Mixture proportions of HSC

Specimen	W/C(%)	S/a(%)	PP fiber (kg/m^3)	Steel fiber (Vol.%)	Mixed ratio(kg/m^3)				
					W	C	F/A	S/F	AD (%)
Ⅰ-25-40-23 (F/A:0%)	35.0	47.0	0.0	0.0	163	466	-	-	1.4
Ⅱ-25-40-23 (F/A:0%)	35.0	47.0	0.5	0.5	163	466	-	-	1.4
Ⅲ-25-50-23 (F/A:0%)	30.0	45.0	0.0	0.0	163	544	-	-	1.4
Ⅳ-25-50-23 (F/A:0%)	30.0	45.0	0.5	0.5	163	544	-	-	1.4
Ⅴ-20-60-23 (F/A:0%)	27.5	45.0	0.0	0.0	163	593	-	-	1.5
Ⅵ- 20-60-23 (F/A:0%)	27.5	45.0	0.5	0.5	163	593	-	-	1.5
Ⅶ-20-80-23 (F/A:10%)	24.9	41.5	0.0	0.0	162	533	65	52	1.9
Ⅷ-20-80-23 (F/A:10%)	24.9	41.5	0.5	0.5	162	533	65	52	1.9
Ⅸ-20-100-23 (F/A:10%)	18.0	33.0	0.0	0.0	145	604	81	121	2.9
Ⅹ-20-100-23 (F/A:10%)	18.0	33.0	1.0	0.5	145	604	81	121	2.9

Table 2 Scope of fire test and analysis

Specimen	Design strength (MPa)	Test strength (28day, MPa)	Test strength	Load (kN)	Load ratio by test strength (28day, %)	Fiber-cocktail	Research scope	
			(56day, MPa)				Test	Analysis
Specimen - Ⅰ (Ⅰ-25-40-23)	40	40.20	45.05	1,219	0.40	×	○	○
Specimen - Ⅱ (Ⅱ-25-40-23)	40	40.20	45.05			○	○	○
Specimen l-Ⅲ (Ⅲ-25-50-23)	50	48.25	52.03	1,414		×	○	○
Specimen -Ⅳ (Ⅳ-25-50-23)	50	48.25	52.03			○	○	○
Specimen - Ⅴ (Ⅴ-20-60-23)	60	56.25	62.01	1,608		×	○	○
Specimen l-Ⅵ (Ⅵ-20-60-23)	60	56.25	62.01			○	○	○
Specimen l-Ⅶ (Ⅶ-20-80-23)	80	72.25	81.03	1,997		×	×	○

Table 2 Continued

Specimen -Ⅷ (Ⅷ-20-80-23)	80	72.25	81.03	2,386	○	×	○
Specimen -Ⅸ (Ⅸ-20-100-23)	100	88.30	98.09		×	×	○
Specimen -Ⅹ (Ⅹ-20-100-23)	100	88.30	98.09		○	×	○

concrete columns were planned using the mixture proportions shown in Table 1. The load ratios shown in Table 2 were calculated by Eq. (1).

$$L.R.(\%) = \gamma(A_sF_y + 0.85A_cf_{ck}) \tag{1}$$

where, $\gamma = 0.4$

As = Cross sectional areas of Main rebar, mm^2

Fy = Yield Strength of Main rebar, MPa

Ac = Cross sectional areas of concrete, mm^2

fck = Compression Strength of concrete, 28day, MPa)

2.2 Material test to obtain input data

Test sample was heated under loading condition in the material test conducted to identify the material properties of the specimen at high temperatures. Table 1 is the mixture proportions and Fig. 1 shows the shape of the test sample and furnace used in the test. Cylindrical test sample was used in the material test at high temperatures.

Table 3 shows thermal expansion properties of the 40~100 MPa high-strength concrete associated with different internal temperatures obtained from the test. Tables 4, 5 and 6 are specific heat property, elastic coefficient and concrete conductivity, respectively. (Kim 2010) The results shown in the tables were used as input data and the data which was not measured at each temperature level was converted to linearly-calculated values for the analysis.

2.3 High-strength concrete column details

The specimens used in the full-scale high-strength concrete column fire test were 270 × 270 × 3000 mm (B × D × L) in dimension. D22 main bars and D10 stirrups made of SD400 steel were placed as shown in Figs. 2 and 5 thermo couples were installed.

3. Fire test of high-strength concrete columns

In order to evaluate the safety of the structural members of high-strength concrete upon a fire, the members should be heated under loading condition in accordance with the ISO 834 fire curve (ISO 834-11999) and the internal temperature, contraction and spalling depth should be measured for the evaluation of fire-resistance performance. This chapter analyzes the thermal characteristics and behavior of the high-strength concrete columns at high temperatures under loading condition shown in Table 2. Under the calculated loading condition, concrete spalling, temperatures

(a) Shape of test sample (b) Furnace of test

Fig. 1 Material test of HSC at high temperatures

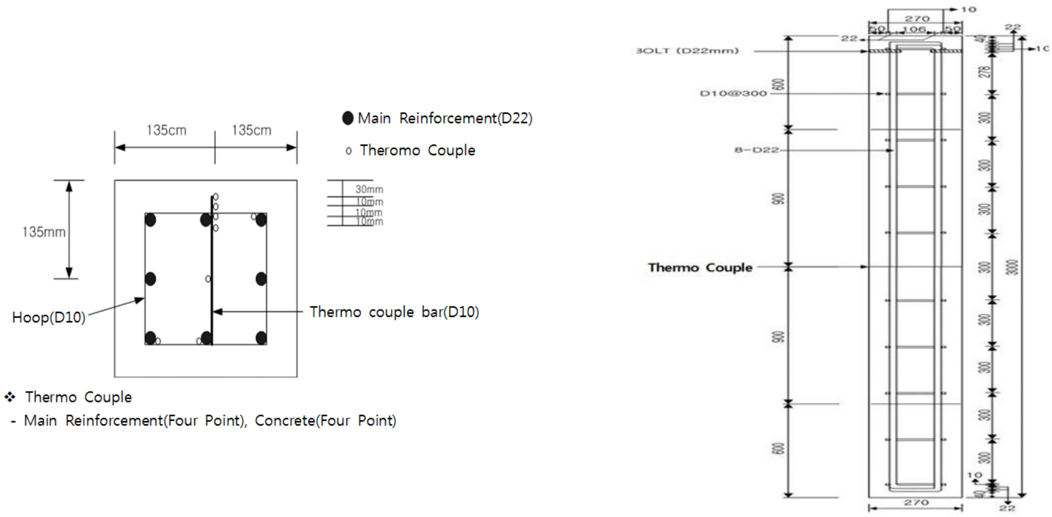

(a) Shape of test sample (b) Furnace of test

Fig. 2 Details of HSC column specimen

at different distances from column surface and column contraction were measured to analyze the fire-resistance performance of the concrete columns. The depth of the most severe spalling was measured. The temperatures of the steel bars and concrete were measured by the thermocouples shown in Fig. 2. The fire resistance requirement applied in Korea is KS F 2257-1 which is in compliance with ISO 834-1. The core of the requirement is as follows: Failure to support the load is deemed to have occurred when both of the following criteria (Eq. (2)) have been exceeded.

Limiting axial contraction, $C = h/100$ mm

$$\text{Limiting rate of axial contraction, } dC/dt = 3h/1000 \text{ mm/min} \tag{2}$$

where, h = initial height of column, mm

3.1 40 MPa concrete columns

In the 40 MPa column without fiber-cocktail, moisture was generated at 5 minute point of heating and it continued to evaporate until 25 minutes (Temperature of main rebar: 114℃). Vertical cracks were observed on the column's surface after 43 minute heating (Temperature of main rebar: 180℃) and partial falling was noticed at 67 minute point (Temperature of main rebar: 240℃). Fig. 3 shows the cracks on the surface observed at 75 minute point (Temperature of main rebar: 288℃). However, the deepest spalling was 15 mm and average spalling depth was 6 mm. The average temperature of main rebar were 516℃ and highest temperature of main rebar were 633℃ at 180 minute point of the test termination, respectively, both of which satisfied fire-resistance requirement.

Before test

After test

Fig. 3 HSC column specimen (40 MPa, Non Fiber -Cocktail)

Table 3 Thermal expansion property of HSC

Temperature (℃)	40MPa (mm × 10^{-8} /℃)		50MPa (mm × 10^{-8} /℃)		60MPa (mm × 10^{-8} /℃)		80MPa (mm × 10^{-8} /℃)		100MPa (mm × 10^{-8} /℃)	
	Ⅰ	Ⅱ	Ⅲ	Ⅳ	Ⅴ	Ⅵ	Ⅶ	Ⅷ	Ⅸ	Ⅹ
20	1102	871	942	972	987	1054	1028	999	1148	992
100	1537	1754	1245	1736	1859	1777	1435	1388	1370	1387
200	2511	2844	1937	2991	3168	2898	2169	2242	1935	2228
300	3552	4099	2755	4490	4761	4257	3084	3275	2667	3547
400	4802	5340	3623	6304	6846	5962	4254	4644	3436	4960
500	9154	8029	6497	11443	12365	10540	8688	9096	7111	10572
600	9377	8951	6663	12146	13134	11665	9365	9392	7068	11280
800	9721	9851	7420	12443	13926	11837	10085	9452	6944	14188

Table 4 Specific heat property of HSC

Temperature (℃)	40MPa (J/kg℃)		50MPa (J/kg℃)		60MPa (J/kg℃)		80MPa (J/kg℃)		100MPa (J/kg℃)	
	Ⅰ	Ⅱ	Ⅲ	Ⅳ	Ⅴ	Ⅵ	Ⅶ	Ⅷ	Ⅸ	Ⅹ
100	497	546	646	609	676	754	-	-	-	-
200	625	551	634	631	683	743	-	738	716	-
300	687	-	713	749	759	-	713	742	-	701
400	721	677	779	-	789	-	729	-	739	725
500	756	789	789	-	832	812	833	825	870	858
600	823	797	-	805	-	-	853	846	-	-
800	843	855	849	831	842	819	0	-	-	-

Table 5 Elastic modulus of HSC

Temperature (℃)	40MPa ($N/mm^2 \times 10^3$)		50MPa ($N/mm^2 \times 10^3$)		60MPa ($N/mm^2 \times 10^3$)		80MPa ($N/mm^2 \times 10^3$)		100MPa ($N/mm^2 \times 10^3$)	
	Ⅰ	Ⅱ	Ⅲ	Ⅳ	Ⅴ	Ⅵ	Ⅶ	Ⅷ	Ⅸ	Ⅹ
20	110.0	104.1	110.0	110.0	110.0	110.0	110.0	110.0	110.0	110.0
100	106.9	105.1	100.8	103.1	100.9	103.3	99.9	101.4	96.7	101.4
200	108.4	108.0	105.0	106.0	102.6	108.4	102.6	106.0	100.3	106.4
300	108.0	108.6	105.4	107.4	106.5	109.1	105.5	106.8	102.8	107.0
400	107.1	107.1	104.2	105.4	105.2	107.3	104.6	105.9	103.0	105.8
500	101.4	103.0	99.6	102.5	99.7	103.8	96.9	99.5	98.1	100.3
600	95.4	97.5	94.2	97.9	96.3	97.0	90.2	95.1	93.5	95.9
800	89.4	91.2	85.5	91.4	88.9	90.6	85.8	89.8	88.0	90.2

Table 6 Concrete conductivity of HSC

Temperature (℃)	40MPa (W/M·K)		50MPa (W/M·K)		60MPa (W/M·K)		80MPa (W/M·K)		100MPa (W/M·K)	
	Ⅰ	Ⅱ	Ⅲ	Ⅳ	Ⅴ	Ⅵ	Ⅶ	Ⅷ	Ⅸ	Ⅹ
20	2.28	2.33	2.18	2.09	2.00	1.94	2.27	1.95	1.81	1.73
100	1.86	1.82	-	2.00	-	1.75	2.03	1.83	1.76	1.70
200	1.65	1.81	1.81	1.7	1.57	1.69	1.9	1.43	1.58	1.46
300	-	-	-	-	-	-	-	-	-	-
400	1.5	1.55	-	1.62	1.56	1.35	1.55	1.25	1.68	1.36
500	-	-	-	-	-	-	-	-	-	-
600	-	1.33	-	-	1.09	1.25	1.44	1.15	1.31	-
800	1.46	1.24	1.77	1.247	-	-	1.37	-	1.2	-

Table 7 Material property of reinforcing-bar at high temperatures (Kim 2002)

Temperature (℃)	Elastic modulus (N/mm^2 $\times 10^3$)	Conductivity (W/M·K)	Expansion coefficient (mm×10^{-8} /℃)	Specific Heat (J/kg℃)
20	214.784	45.563	1220	440.4
119	208.680	42.305	-	456.1
205	189.343	42.634	1270	500.2
306	186.153	40.527	1310	542.1
411	192.510	39.758	1350	611
514	134.255	37.806	1400	682.8
617	111.282	34.849	1440	786.7
718	45.244	48.657	1490	-
817	56.930	43.305	-	1015.3
913	38.572	53.448	-	1089.7

Table 8 Material property of steel fiber (Kim 2002)

Elastic modulas (N/mm^2)	Specific gravity	Fiber length (mm)	Tensile strength (MPa)	Ultimate elongation (%)
200,000	7.85	30	1,100	3.5

Table 9 Material property of pp fiber (Kim 2002)

Type	Shape	Specific gravity	Melting point (℃)	Ignition point(℃)	Tensile elastic modulas(MPa)
PM Type	Homopolymer	0.91	162	3.5	350~770

Before test

After test

Fig. 4 HSC column specimen (50 MPa, Non fiber -cocktail)

Before test After test

Fig. 5 HSC column specimen (50 MPa, fiber-cocktail)

3.2 50 MPa concrete column

3.2.1 Column without fiber-cocktail

In the column, the rupture of the aggregate which began after 5 minute heating was immediately followed by spalling and moisture evaporation and falling progressed simultaneously. The thermal expansion of the heated concrete and the increase in load caused the falling of the concrete surface at the upper part of the column and exposed steel bars were severely deformed due to the heat and load as shown in Fig. 4. The deepest spalling was 92 mm and the average depth of the spalling was 40~50 mm.

3.2.2 Column with fiber-cocktail

In both of the columns with and without fiber-cocktail, the rupture of the aggregate which began after 5 minute heating was immediately followed by spalling and water evaporation and surface falling progressed simultaneously. In the column with fiber-cocktail, however, spalling was concentrated in the center and concrete falling was severe than spalling. Due to thermal expansion and the increase in load, concrete surface at the center of the column fell off. The deepest spalling was 60 mm and the average spalling depth was 20~30 mm. Both the maximum and average depths were less than those of the columns without fiber-cocktail by approximately 30 mm. The average spalling depth, in particular, was less than 50 mm, the distance between column surface and reinforcing-bars as shown in Fig. 6

3.3 60MPa concrete column

3.3.1 Column without fiber-cocktail

In the 60 MPa column without fiber-cocktail, the rupture of the aggregate which began after 5 minute heating was immediately followed by spalling. Concrete falling and spalling were generated together at 18 minute point (Temperature of main rebar: 124℃) and water was drawn to the column surface and trickled down due to the rapid spout of moisture. Concrete spalling accompanying concrete falling and aggregate rupture was observed on all of the 4 planes of the

Before test After test

Fig. 6 HSC Column specimen (60 MPa, NON Fiber-Cocktail)

Before test After test

Fig. 7 HSC Column specimen (60 MPa, Fiber-Cocktail)

column after 12 minutes (Temperature of main rebar: 86.6℃) and continued to progress until 25 minute point (Temperature of main rebar: 220.9℃) to make the steel bars exposed in all of the planes. The deepest spalling was 73.47 mm and the average spalling depth was 59.95 mm as shown in Fig. 6.

3.3.2 Colum with fiber-cocktail

In the column with fiber-cocktail, concrete falling began at the central part after 5 minute heating. Water-trickling caused by rapid spout of moisture was observed at 20 minute point (Temperature of main rebar: 107℃) and continued to progress until 30 minutes (Temperature of main rebar: 158.7℃) to result in severe concrete falling at the centers of all of the 4 surfaces as shown in Fig. 7.

Concrete spalling was observed only at the central part of the column. The deepest spalling was

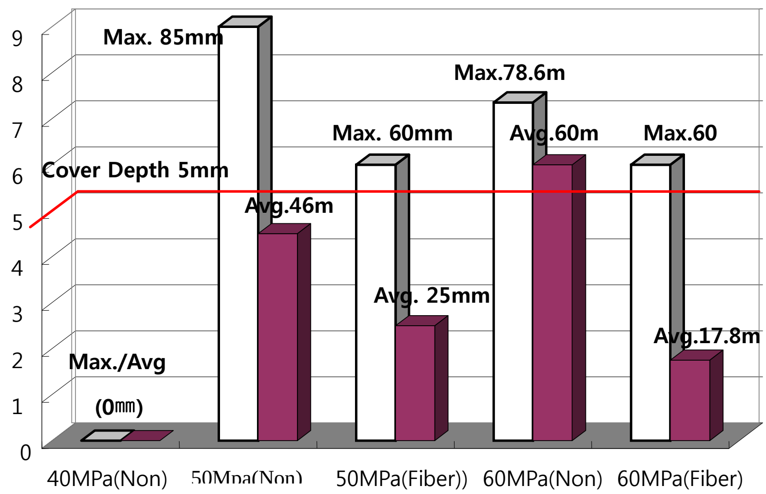

Fig. 8 Spalling effect compare mixing-fiber cocktail with non mixing fiber - cocktail of HSC

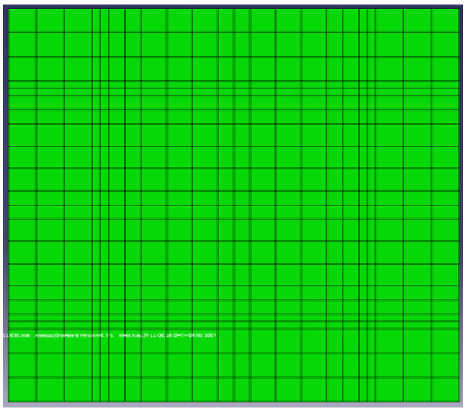

(a) Mesh of concrete part

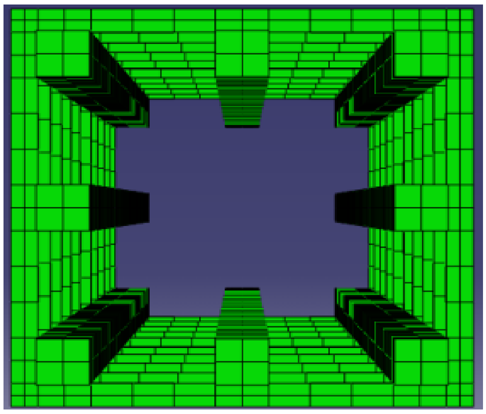

(b) Mesh of reinforcement.

Fig. 9 Analysis model geometry

Table 10 Evaluation of fire resistance performance by ISO 834-1

Strength	Fiber cocktail	Maximum rate of axial contraction (mm/min)	Maximum axial contraction (mm)	Fire resistance (Minute)	Temperature (℃)	
					Ava.	Max.
40MPa	×	8.6	15.5	180	516	633
	○	7.3	10.1	180	382	390
50MPa	×	19.2	45.2	130	436	759
	○	62.5	56.0	168	472	740
60MPa	×	65.0	78.0	103	435	887
	○	29.0	39.7	138	362	566

60 mm and the average spalling depth was 20 mm which was significantly less than 50 mm, the distance between the column surface and steel bars and less than that measured in the column without fiber-cocktail by approximately 40 mm. It is deduced that micro pores generated by the dissolution of the fiber enabled the pore pressure and vapor to spout effectively and thus controlled spalling and temperature rise.

3.4 Analysis of spalling & fire-resistance associated with fiber-cocktail

While spalling was observed in the columns of 40 MPa concrete which is classified as high-strength concrete in Korean specification, it was not severe enough to threaten the structural safety of the members upon a fire.

The rupture of the aggregate observed after 5 minute heating accompanied spalling in 50 and 60 MPa concrete columns with fiber-cocktail as in those without fiber-cocktail, but the spalling in the former was less severe than in the latter by 20~40 mm. The mitigation of spalling enabled by the fiber-cocktail was more effective in 60 MPa concrete than in 50 MPa concrete. Fig. 8 shows the comparison of the spalling in the high-strength concrete columns with and without fiber-cocktail.

40 MPa concrete column without fiber-cocktail was not deformed severely enough to cause structural collapse, which determines that it satisfies the fire-resistance for 180 minutes required by ISO 834-1. However, in 50 and 60MPa columns, heat-generated concrete expansion and load pressure at the beginning of heating caused concrete spalling at upper parts and deformed the steel bars rapidly. They resisted fire for 130 and 103 minutes, respectively, which were shorter than the requirement by 50 and 77 minutes, respectively. Table 10 summarizes evaluation of the fire resistance by ISO.

4. FE input data

4.1 Analysis condition

The fire scenario used in the test and analysis in this study was the standard building fire of the ISO 834, a heating curve based on the “cellulose fire”. Eq. (3) shows its typical temperature rise pattern. In the analysis based on the fire-resistance requirement of 3 hours, the commercial program of ABAQUS was used..

$$\text{Temperature } (^\circ\text{C}) = 20 + 345 \times \text{LOG}\,(8 \times \text{time}+1) \tag{3}$$

Eq. (4) is the heat transfer equation for the analysis where the element model of DC3D8 was used.

$$q = \alpha_c\,(\theta_g-\theta_m)^m + V_\sigma\,(\alpha_m\varepsilon_f\theta_m^4-\varepsilon_f\theta_m^4) \tag{4}$$

where α_c: Thermal convection coefficient (Fire exposure condition of 7 W/m^{2}Km)

m: Thermal convection generation coefficient (1.0, Surface exposed to a fire)

θ_g: Furnace temperature (K)

θ_m: Model temperature (K)

V: Radiant angle coefficient (1.0)

E_f: Flame (furnace) heat emission rate (= 0.7)
E_m: Model heat emission rate (= 0.8)
A_m: Surface absorption rate
σ: Stefan-Boltzmann constant (=5.67×10^{-8} W/m^{2}K^4)

The analysis in this study was conducted to see if the concrete columns being used in Korea satisfy the fire-resistance performance requirement and covered the prediction of steel bar temperatures inside the concrete columns and their axial deformation only. Table 11 shows the fire-resistance standard for the concrete columns and Table 12 shows the plan of fire analysis.

The result of material test associated with each temperature level was used as the input data for the analysis of the high-strength concrete (80~90 MPa). In order to predict the temperature and column contraction in accordance with the ISO 834 fire, specific heat, heat convection rate and heat expansion rate derived from the test of the materials having the identical mixture proportions with the specimens were used in the analysis.

The assumption in the analysis is as follows. Fig. 9 is the analysis model geometry with the meshes 30 mm^2 in dimension.

▪ The longitudinal planes of the high-strength concrete columns are equally exposed to the standard fire and heat transfer along z-axis does not occur. The concrete surfaces which are directly exposed to the fire are perfectly plane. Therefore, heat transfers only along the planes (X and Y axes).

▪ The connection between the steel bars and concrete is complete connection, so heat transfer or the change in heat flux does not exist in the connection.

Table 11 KS F 2257-1 standard for concrete column

Temperature of reinforcing bar	Deformation of column
Average : 538℃, Max : 649℃	H/30

Table 12 Plan of fire analysis

Model	Strength (MPa)	Fiber cocktail	Comparion plan		
			Research scope		Comparision condition
			Fire test	Analysis	
Ⅰ	40	×	○	○	Test & Analysis
Ⅱ	40	○	○	○	Test & Analysis
Ⅲ	50	×	○	○	Test & Analysis
Ⅳ	50	○	○	○	Test & Analysis
Ⅴ	60	×	○	○	Test & Analysis
Ⅵ	60	○	○	○	Test & Analysis
Ⅶ	80	×	×	○	prediction
Ⅷ	80	○	×	○	prediction
Ⅸ	100	×	×	○	prediction
Ⅹ	100	○	×	○	prediction

4.2 Comparison between numerical analysis and fire test

4.2.1 Comparison of temperature changes (Model- I ~ VI)

The results for model I ~ VI obtained from the test and analysis were compared to verify the reliability of the analysis method for the prediction of the heat transfer and behavior characteristics of the high-strength concrete. Analysis result was compared with the result measured by the thermo couples installed at a distance of 30, 40 and 50 mm from the concrete column surface. The test of model I was conducted for 180 minutes, while those of model III and model V were terminated after 130 and 105 minutes, respectively and the analysis was made for the same period of time with the test. As shown in Figs. 10~12, the analysis and test provided relatively similar results.

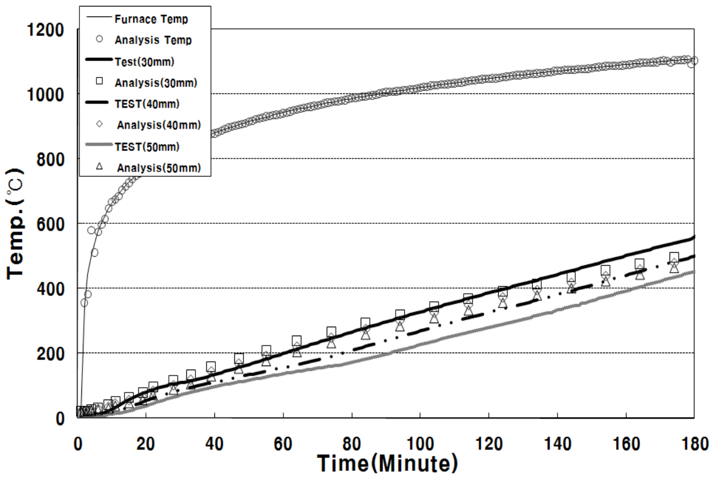

Fig. 10 Comparison between test and analysis (Model-Ⅰ)

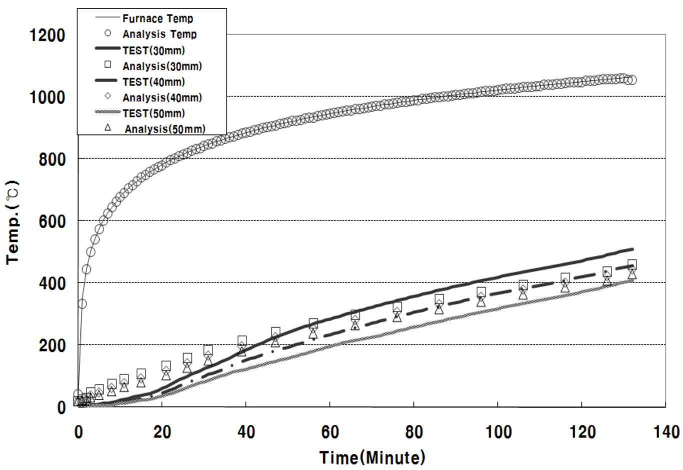

Fig. 11 Comparison between test and analysis (Model-Ⅲ)

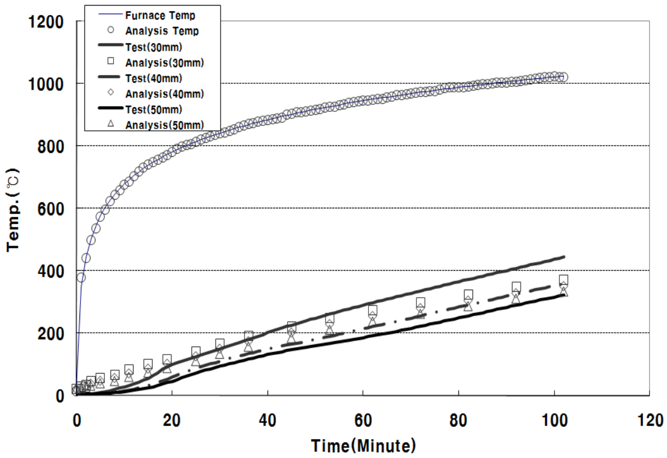

Fig 12 Comparison between test and analysis (Model-Ⅴ)

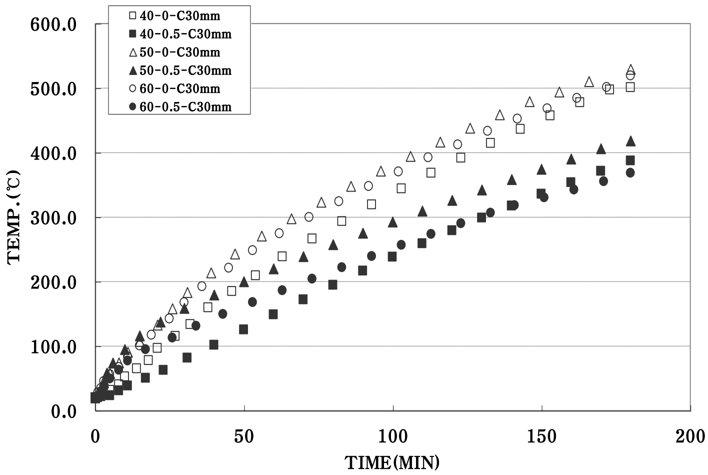

Fig 13 Comparison between test and analysis (Model-Ⅰ,Ⅲ,Ⅴ)

Table 13 Result of heat transfer analysis

Model	Strength (MPa)	Fiber cocktail	Temperature (180 Minute)				
			Concrete (℃)				Reinforced bar (℃)
			0 mm	30 mm	40 mm	50 mm	
Ⅰ	40	×	612	501	484	467	428
Ⅱ	40	○	516	387	376	364	384
Ⅲ	50	×	638	529	514	501	484
Ⅳ	50	○	488	418	407	398	355
Ⅴ	60	×	669	519	498	492	459
Ⅵ	60	○	482	368	357	334	326

In order to compare the heat transfer characteristics associated with concrete strength and fiber-cocktail, the temperatures at 30 mm from the surface were compared. It was observed that the increase in concrete strength accelerated temperature rise but the influence was not material. However, since the use of fiber-cocktail had an influence on the heat convection rate and specific heat of the column, it controlled heat transfer by approximately 100℃. Fig. 12 shows the result.

Since the melting point of the polypropylene fiber is low, micro cracks are generated when exposed to high temperatures through which heat and vapor spout out of the column. In addition, the proper use of steel fiber offsets the rupture stress caused by micro cracks and explosive spalling and prevents the damage to the planes.

Table13 shows the results of heat transfer analysis. The maximum temperatures in model I and II were 428 and 384℃, respectively seemingly because the dissolution of the fiber generated micro pores in the concrete and the heat spouted out of the concrete through the pores effectively.

4.2.2 Comparison of column deformation (Model-Ⅰ~Ⅵ)

The properties of the members at high temperatures such as thermal expansion rate and modulus of elasticity obtained from the material test were applied to thermal stress analysis to predict column deformation. As shown in Fig. 14, the analysis and test provided similar results in terms of column deformation. Since the regulation for fire tests (KS F1157-1) prescribes that the test should be terminated when the displacement reaches H/100, the numerical analysis was conducted for the maximum of 180 minutes to predict the deformation characteristics of the columns exposed to high temperatures, which can not be accomplished by a test.

The analysis of column contraction associated with concrete strength in the columns without fiber-cocktail showed that deflection was generated earlier in the columns with higher strength. It was because the higher axial load leads to acceleration of deterioration rate of high strength concrete columns associated with spalling and higher temperature distributions.

The fire-resistance performance of the columns with fiber-cocktail was superior to that of those without fiber-cocktail thanks to less severe column contraction. Fig. 14 shows the displacement of the models associated with concrete strength and fiber-cocktail. It is because the specific heat of the concrete with fiber-cocktail below 400℃ was higher than that without fiber-cocktail and the thermal expansion rate and heat conductivity of the former were lower than those of the latter

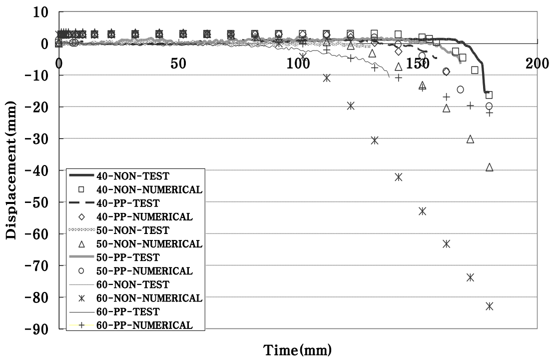

Fig. 14 Comparison between test and analysis under loading condition (Model-Ⅰ~Ⅵ)

in the material test. Therefore, temperatures were lower and deformation was less severe in the concrete columns with fiber-cocktail when compared with those without fiber-cocktail.

The comparison between the analysis result and test result decided that the analysis method used to predict the heat transfer characteristics of the concrete columns and axial deformation of the columns without fiber-cocktail is reliable. In less than 50 MPa concrete columns with fiber-cocktail, the two results were also similar to each other. However, as shown in Table 14, there was a difference of approximately 42 minutes between the analysis and test results in terms of the fire-resistance of model VI with fiber-cocktail. It was seemingly because the thermal expansion rate of the sample specimen with fiber-cocktail in the material test was less than that of actual column structure.

4.3 Prediction of heat transfer & behavior of high-strength concrete columns upon a fire

4.3.1 Prediction of heat transfer (Model-Ⅶ～Ⅹ)

It was found in the analysis that the temperature under the ISO 834 fire condition for 180 minutes was lower by approximately 120℃ when fiber-cocktail was employed in the concrete columns, which showed that the fiber-cocktail controlled heat transfer. No significant difference in temperature was predicted in association with concrete strength as shown in Fig. 15.

4.3.2 Prediction of the behavior upon a fire (Model-Ⅶ～Ⅹ)

The numerical analysis conducted to predict the deformation of high-strength concrete upon a fire showed that the deflection of the models without fiber-cocktail was greater than those with fiber-cocktail by approximately 70 mm as shown in Fig. 16. It is because of the thermal stress and thermal expansion caused by the temperature difference of about 120℃ in the heat transfer analysis conducted in 4.2.1. However, since the deterioration in stiffness can be possibly experienced in the high-strength concrete with fiber-cocktail, it is required to develop the mixture proportion to solve this problem in order to secure the fire-resistance for 180 minutes.

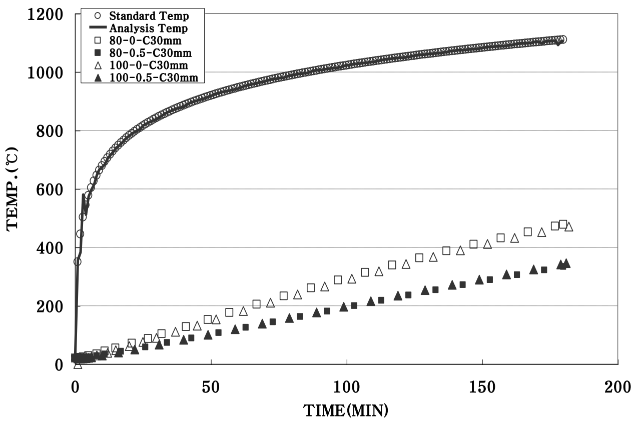

Fig 15 Prediction to heat transfer (Model-Ⅶ～Ⅹ)

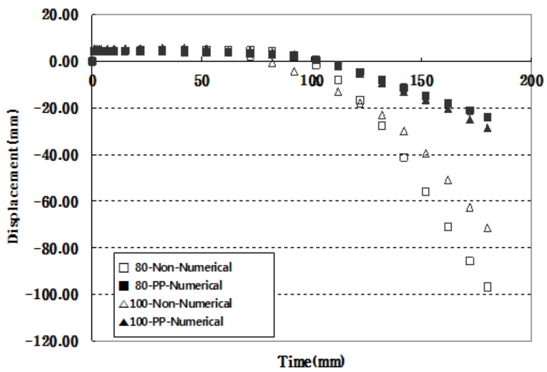

Fig. 16 Prediction to column behaviour (Ⅶ~Ⅹ)

Table 14 Result of fire behavior analysis

Model	Strength	Fiber cocktail	Maximum rate of axial contraction (mm/min)	Maximum axial contraction (mm)	Fire resistance (Minute)	
					Test	Analysis
Ⅰ	40MPa	×	1.306	16.5	180	180
Ⅱ		○	0.49	9	180	180
Ⅲ	50MPa	×	1.133	41	130	131
Ⅳ		○	0.67	21	168	180
Ⅴ	60MPa	×	1.16	83	103	102
Ⅵ		○	0.32	22	138	180

5. Conclusions

In this study, tests were conducted to investigate the spalling of high-strength concrete columns with and without fiber-cocktail. In addition, numerical analysis was made to predict the fire-resistance of the concrete columns based on Korean standards and the result was compared with the test result. The conclusion is as follows.

1. The use of fiber-cocktail (PP - 0.5 kg/m^3, steel fiber 0.5 %/VOL) can control the spalling of 50 and 60MPa high-strength concrete columns by 20~40 mm, on average.

2. The deformation of the columns with fiber-cocktail under standard fire condition was less than that of the columns without fiber-cocktail by approximately 25~55 %, which constitutes the improvement in fire-resistance performance.

3. The fire-resistance performance of the columns with fiber-cocktail is improved because the lower melting point of polypropylene fiber enables micro cracks through which heat and vapor can spout out of the column when exposed to high temperatures and the steel fiber in the columns simultaneously controls the micro cracks and offsets the rupture stress caused by explosive spalling and thus prevents the damage to the planes.

4. In predicting the fire-resistance under unloaded condition, the temperature inside members

should not exceed the limit (649℃). The fire-resistance analysis of the analysis models based on the standard showed that the temperatures of model V, VII and IX exceeded the limit under the standard fire condition for 180 minutes.

5. In the analysis, models V and VI and models VII and VIII showed similar behaviors until 140 minute point. Then, the column displacement of model VII increased to reach axial deformation of 96.8 mm.

Acknowledgements

This study was conducted as part of the KICT's project "[13] Structures have more than 3 hour fire-resistance rating where building have floor area of 3,000 m^2 of more(10 m, without fire-proofing) and soke control·evacuation(1.8 m smoke layer height) technology development " sponsored by the Korean Ministry of Knowledge Economy. The authors of this paper are grateful for the supports.

References

Abaqus (2004), Theory Manual, Version 5.8, Hibbit, Karlsson & Sorensen Inc.

Bažant, Z.P. and Bhat, P.D. (1976), "Endochronic theory of inelasticity and failure of concrete", *ASCE J. Eng. Mech.*, **102**(4), 701-722.

Bažant, Z.P. and Ožbolt, J. (1990), "Non-local microplane model for fracture, damage and size effect in structures", *ASCE J. Eng. Mech.*, **116**(11), 2485-2505.

Bažant, Z. and Planas, J. (1998), Fracture and size effect in concrete and other quasi-brittle materials, CRC Press LLC.

Bažant, Z.P. and Jirásek, M. (2002), "Numerical integral formulations of plasticity and damage: survey of progress", *ASCE J. Eng. Mech.*, **128**(11), 1119-1149.

Bobiński, J. and Tejchman, J. (2004), "Numerical simulations of localization of deformation in quasibrittle materials within non-local softening plasticity", *Comput. Concrete*, **1**(4), 1-22.

Bobiński, J. and Tejchman, J. (2013), "A coupled continuous-discontinuous approach to concrete elements". *Proc. Int. Conf. Fracture Mechanics of Concrete and Concrete Structures FraMCoS-8 (eds.: J. G. M. van Mier, G. Ruiz, C. Andrade, R. C. Yu, X. X. Zhang)*.

Brinkgreve, R.B.J. (1994), "Geomaterial models and numerical analysis of softening", Ph.D. Thesis, Delft University of Technology, Delft.

Carol, I. and Willam, K. (1996), "Spurious energy dissipation/generation in stiffness recovery models for elastic degradation and damage", *Int. J. Solids Struct.*, **33**(20-22), 2939-2957.

Cervenka, J. and Papanikolaou, V.K. (2008), "Three dimensional combined fracture-plastic material model for concrete", *Int. J. Plasticity*, **24**(12), 2192–2220.

Committé Euro-International du Béton, (1991), "CEB-FIP model code 1990: design code", *Bulletin d'information*, 213-124.

de Borst, R. and Nauta, P. (1985), "Non-orthogonal cracks in a smeared finite element model", *Eng. Comput.*, **2**(1), 35-46.

de Borst, R. (1986), "Non-linear analysis of frictional materials", Ph.D. Thesis, University of Delft, Delft.

de Borst, R., Pamin, J. and Geers, M. (1999), "On coupled gradient-dependent plasticity and damage theories with a view to localization analysis", *Eur. J. Mech. A/Solids*, **18**(6), 939-962.

de Vree J.H.P., Brekelmans W.A.M. and van Gils, M.A.J. (1995), "Comparison of non-local approaches in continuum damage mechanics", *Comput. Struct.*, **55**(4), 581-588.

den Uijl, J.A. and Bigaj, A. (1996), "A bond model for ribbed bars based on concrete confinement", *Heron*,

41(3), 201-226.
Dörr, K. (1980), Ein Beitag zur Berechnung von Stahlbetonscheiben unter Berücksichtigung des Verbundverhaltens, Phd Thesis, Darmstadt University, Darmstadt.
Dragon, A. and Mróz, Z. (1979), "A continuum model for plastic-brittle behaviour of rock and concrete", *Int. J. Eng. Sci.*, **17**(2), 121-137.
Geers, M.G.D. (1997), Experimental analysis and computational modeling of damage and fracture, PhD Thesis, Eindhoven University of Technology, Eindhoven.
Gitman, I.M., Askes, H. and Sluys, L.J. (2008), "Coupled-volume multi-scale modelling of quasi-brittle material", *Eur. J. Mech. A/Solids*, **27**(3), 302-327.
Haskett, M., Pehlers, D.J. and Mohamed Ali, M.S. (2008), "Local and global bond characteristics of steel reinforcing bars", *Eng. Struct.*, **30**(2), 376-383.
Häuβler-Combe, U. and Pröchtel, P. (2005), "Ein dreiaxiale Stoffgesetz fur Betone mit normalen und hoher Festigkeit", *Beton- Stahlbetonbau*, **100**(1), 56-62.
Hordijk, D.A. (1991), Local approach to fatigue of concrete, PhD Thesis, Delft University of Technology, Delft.
Hsieh, S.S., Ting, E.C. and Chen, W.F. (1982), "Plasticity-fracture model for concrete", *Int. J. Solids Struct.*, **18**(3), 181-187.
Hughes, T.J.R. and Winget, J. (1980), "Finite Rotation Effects in Numerical Integration of Rate Constitutive Equations Arising in Large Deformation Analysis", *Int. J. Numer. Methods Eng.*, **15**(12), 1862-1867.
Ibrahimbegovic, A., Markovic, D. and Gatuing, F. (2003), "Constitutive model of coupled damage-plasticity and its finite element implementation", *Eur. J. Finite Elem.*, **12**(4), 381-405.
Jirásek, M. and Zimmermann, T. (1998), "Analysis of rotating crack model", *ASCE J. Eng. Mech.*, **124**(8), 842-851.
Jirásek, M. (1999), "Comments on microplane theory", *Mechanics of quasi-brittle materials and structures (eds.: G. Pijaudier-Cabot, Z. Bittnar and B. Gerard), Hermes Science Publications*, 55-77.
Jirásek, M. and Marfia, S. (2005), "Non-local damage model based on displacement averaging", *Int. J. Numer. Methods Eng.*, **63**(1), 77-102.
Lee, J. and Fenves, G.L. (1998), "Plastic-damage model for cyclic loading of concrete structures", *ASCE J. Eng. Mech.*, **124**(8), 892-900.
Lorrain, M., Maurel, O. and Seffo, M. (1998), "Cracking behaviour of reinforced high-strength concrete tension ties", *ACI Struct. J.*, **95**(5), 626-635.
Majewski, T., Bobiński, J. and Tejchman, J. (2008), "FE-analysis of failure behaviour of reinforced concrete columns under eccentric compression", *Eng. Struct.*, **30**(2), 300-317.
Mahnken, R. and Kuhl, E. (1999), "Parameter identification of gradient enhanced damage models", *Eur. J. Mech. A/Solids*, **18**(5), 819-835.
Marzec, I., Bobiński, J. and Tejchman, J. (2007), "Simulations of crack spacing in reinforced concrete beams using elastic-plasticity and damage with non-local softening", *Comput. Concrete*, **4**(5), 377-403.
Marzec, I. and Tejchman, J. (2012), "Enhanced coupled elasto-plastic-damage models to describe concrete behaviour in cyclic laboratory tests: comparison and improvement", *Arch. Mech.*, **64**(3), 227–259.
Mazars, J. (1986), "A description of micro- and macroscale damage of concrete structures", *Eng. Fract. Mech.*, **25**(5-6**)**, 729-737.
Menetrey, P. and Willam, K.J. (1995), "Triaxial failure criterion for concrete and its generalization", *ACI Struct. J.*, **92**(3), 311-318.
Meschke, G. and Dumstorff, P. (2007), "Energy-based modeling of cohesive and cohesionless cracks via X-FEM", *Comput. Meth. Appl. Mech. Eng.*, **196**(21-24), 2338-2357.
Moonen, P., Carmeliet, J. and Sluys, L.J. (2008), "A continuous-discontinuous approach to simulate fracture processes", *Philos. Mag.*, **88**(28-29), 3281-3298.
Oliver, J. and Linero, D.L. and Huespe, A.E. and Manzoli, O.L. (2008), "Two-dimensional modeling of material failure in reinforced concrete by means of a continuum strong discontinuity approach", *Comput. Meth. Appl. Mech. Eng.*, **197**(5), 332-348.

Ooi, E.T. and Yang, Z.J. (2011), Modelling crack propagation in reinforced concrete using a hybrid finite element–scaled boundary finite element method", *Eng. Fract. Mech.*, **78**(2), 252-273.
Pamin, J. and de Borst, R. (1999), "Stiffness degradation in gradient-dependent coupled damage-plasticity", *Arch. Mech.*, **51**(3-4), 419-446.
Peerlings, R.H.J., de Borst, R., Brekelmans, W.A.M. and Geers, M.G.D. (1998), "Gradient enhanced damage modelling of concrete fracture", *Mech. Cohes.-Frict. Mat.*, **3**(4), 323-342.
Pietruszczak, S., Jiang, J. and Mirza, F.A. (1988), "An elastoplastic constitutive model for concrete", *Int. J. Solids Struct.*, **24**(7), 705-722.
Pijaudier-Cabot, G. and Bažant, Z.P. (1987), "Nonlocal damage theory", *ASCE J. Eng. Mech.*, **113**(10), 1512-1533.
Rabczuk, T. and Zi, G. and Bordas, S. and Nguyen-Xuan, H. (2008), "A geometrically non-linear three-dimensional cohesive crack method for reinforced concrete structures", *Eng. Fract. Mech.*, **75**(16), 4740-4758.
Ragueneau, F., Borderie, C.H. and Mazars, J. (2000), "Damage model for concrete-like materials coupling cracking and friction", *I. J. Num. Anal. Meth. Geomech.*, **5**(8), 607-625.
Rots, J. G. and Blaauwendraad, J. (1989), "Crack models for concrete, discrete or smeared? Fixed, multi-directional or rotating?", *Heron*, **34**(1), 1-59.
Simo, K.C. and Ju, J.W. (1987), "Strain- and stress-based continuum damage models - I. Formulation", *Int. J. Solids Struct*,. **23**(7), 821-840.
Simone, A. and Sluys, L.J. (2004), "The use of displacement discontinuities in a rate-dependent medium", *Comput. Meth. Appl. Mech. Eng.*, **193**(27-29), 3015-3033.
Skarżyński, Ł. and Tejchman, J. (2010), "Calculations of fracture process zones on meso-scale in notched concrete beams subjected to three-point bending", *Eur. J. Mech. A/Solids*, **29**(4), 746-760.
Skarżynski, L, Syroka, E. and Tejchman, J. (2011), "Measurements and calculations of the width of the fracture process zones on the surface of notched concrete beams", *Strain*, **47**(s1), 319-332.
Sluys, L.J. and de Borst, R. (1994), "Dispersive properties of gradient and rate-dependent media", *Mech. Mater.*, **18**(2), 131-149.
Souza, R.A. (2010), "Experimental and numerical analysis of reinforced concrete corbels strengthened with fiber reinforced polymers", *Computational Modelling of Concrete Structures*, (Eds. Bicanic, N., de Borst, R., Mang, H. and Meschke, G.), Taylor and Francis Group, London, 711-718.
Syroka, E., Bobiński, J. and Tejchman, J. (2011), "FE analysis of reinforced concrete corbels with enhanced continuum models", *Finite Elem. Anal. Des.*, **47**(9), 1066-1078.
Syroka-Korol, E. (2012), "Experimental and theoretical investigations of size effects in concrete and reinforced concrete beams", Ph.D. Thesis, Gdańsk University of Technology, Gdańsk
Tejchman, J. and Bobiński, J. (2013), *Continuous and discontinuous modeling of fracture in concrete using FEM*, Springer, (Eds. Wu, W. and Borja, R.I.), Berlin-Heidelberg, Germany.
Walraven, J. and Lehwalter, N. (1994), "Size effects in short beams loaded in shear", *ACI Struct. J.*, **91**(5), 585-593.

CC